Saudi Journal of Chemistry and Materials Science
(*Saudi J. Chem. Mater. Sci.*)
https://www.saudipublications.com/index.php/sjcm/index

Modular Synthesis, Tautomeric Chelate Ring Stabilization, and Dual-Emission Photophysics of Functionalized 3,4-Dihydrocinnolin-4(1*H*)-one Fluorophores

Mahmoud M. Sultan[1,*], **Mohammed G. Assy**[1], **Wael Shehta**[1], **Samar El-Kalyoubi**[2], **Eman Abd Alsalam**[3]

[1] *Department of Chemistry, Faculty of Science, Zagazig University, Zagazig 44519, Egypt.*

[2] *Department of Pharmaceutical Organic Chemistry, Faculty of Pharmacy, Port Said University, Port Said, Egypt.*

[3] *High Technological Institute for Applied Health Sciences, K 36 Cairo–Ismailia Road, Cairo, Egypt.*

ABSTRACT

A modular, metal-free, and atom-economical synthetic strategy has been established for the divergent preparation of structurally functionalized 3,4-dihydrocinnolin-4(1H)-one fluorophores (2–11). The approach utilizes the bifunctional diazo linchpin (E)-2-((1-cyano-2-ethoxy-2-oxoethyl)diazenyl)benzoic acid (1), which undergoes base-catalyzed tandem cyclocondensation with diverse active methylene synthons and primary amine nucleophiles to furnish the target heterocycles in good to high isolated yields (64–85%). A stepwise reaction mechanism is proposed, encompassing intermolecular nucleophilic addition, intramolecular acyl substitution, dehydration, and keto–enol tautomerism. Molecular structures were verified by FT-IR, 1D NMR (1H and 13C), EI-MS, and elemental microanalyses. Diagnostic 1H-NMR spectra exhibited a characteristic downfield resonance at δ 15.22–16.69 ppm, confirming an intramolecularly hydrogen-bonded keto–enol / lactam–lactim equilibrium that establishes a quasi-aromatic S(6) chelate ring via resonance-assisted hydrogen bonding (RAHB). Photophysical measurements in ethanol at 298 K revealed localized π→π transitions at 265.0 nm alongside broad intramolecular charge transfer (ICT) bands between 365.1 and 395.0 nm. Selective photoexcitation into the ICT manifold produces cyan-to-blue fluorescence (λem = 467.0–486.6 nm), with emission intensity governed by C-3 substituent electronics and planarity—reaching 8516 counts for the 3-acetyl analogue 8 (R-507) and 7078 counts for the 3-benzothiazolyl derivative 9 (R-508). Secondary emission bands (508.6–533.0 nm) in compounds 2 (R-501), 5 (R-504), and 9 (R-508) indicate coupled excited-state intramolecular proton transfer (ESIPT) and twisted intramolecular charge transfer (TICT) relaxation pathways. The fluorophores exhibit large Stokes shifts spanning 72.0 to 104.3 nm (up to 143.5 nm for secondary phototautomer bands), effectively eliminating spectral self-absorption. Collectively, these attributes highlight functionalized 3,4-dihydrocinnolin-4(1H)-ones as promising candidate scaffolds for future development in luminescent probes and optoelectronic materials.*

Keywords: *3,4-Dihydrocinnolin-4(1H)-one; Divergent cyclocondensation; Reaction mechanism; Intramolecular charge transfer (ICT); Excited-state intramolecular proton transfer (ESIPT); Dual luminescence; Stokes shift; Optoelectronic prospects.*

1. Introduction

Nitrogen-containing heterocyclic architectures represent fundamental structural motifs across synthetic chemistry, serving as critical platforms in medicinal therapeutics, molecular pharmacology, and photonic materials [1–4]. Within the family of ortho-fused diaza-heterocycles, cinnoline (1,2-diazanaphthalene) frameworks and their oxidized 4-oxo congeners hold a distinctive role owing to their rigid planar geometry, thermodynamic resilience, and tunable supramolecular recognition profiles [5,6]. Recognized as diaza-bioisosteres of quinolines, isoquinolines, and quinazolines, cinnolinone derivatives display notable bioactivities encompassing antimicrobial, antifungal, anti-inflammatory, and selective antitumor properties, alongside emerging applications as kinase inhibitors and central nervous system modulators [7–10]. Beyond pharmacological frontiers, the electron-deficient diaza nucleus, extended π-conjugation, and customizable dipole moments of cinnolinones have catalyzed substantial interest in materials chemistry, establishing them as promising candidates for dye-sensitized solar cells (DSSCs), organic semiconducting layers, and luminescent chemical sensors [11–13].

Simultaneously, the expansion of advanced photonic technologies—including high-resolution fluorescence bioimaging, environmental analyte detection, and organic light-emitting devices (OLEDs)—has accelerated the pursuit of tailor-made small-molecule organic fluorophores [14–17]. Realizing high analytical fidelity in these applications necessitates chromophores characterized by efficient Intramolecular Charge Transfer (ICT) or Excited-State Intramolecular Proton Transfer (ESIPT) dynamics coupled with large Stokes shifts (>80 nm) [18–20]. Planar fluorophores with small Stokes shifts (<40 nm) frequently suffer from radiative loss caused by

Corresponding author emails: Moslem_205@yahoo.com (**Mahmoud M. Sultan**)
Doi: https://doi.org/10.5281/SJCMS2026.1.1.32 ***Saudi J. Chem. Mater. Sci., 1 (1), 97-112 (2026)***
Received Date: 23 October 2026. Revised date: 19 November 2026. Accept Date: 23 November 2026

spectral self-overlap (the inner-filter effect) and concentration-dependent aggregation-caused quenching (ACQ) in condensed phases [21,22]. Expanding the Stokes shift through excited-state structural relaxation—such as keto–enol phototautomerization or twisted intramolecular charge transfer (TICT)—effectively decouples the absorption envelope from radiative emission. This spectral divergence eliminates optical self-absorption, minimizes background interference, and markedly enhances signal-to-noise ratios in demanding optical regimes [23,24].

Despite the compelling optoelectronic potential of cinnolin-4(1H)-one cores, their systematic development has historically been curtailed by synthetic limitations [25,26]. Traditional routes toward cinnoline skeletons—including the classical Richter, Widman–Stoermer, Neber–Bossert, and Borsche reactions—routinely demand corrosive acid media, prolonged high temperatures, or complex multi-step precursors prone to narrow functional group compatibility and modest cumulative yields [27–30]. More recent catalytic and microwave-assisted protocols have improved access to 3-substituted cinnolines [31,32], yet they generally yield fully aromatic systems or require specialized metal catalysts such as InCl3. Furthermore, existing methods rarely allow divergent entry into densely substituted 3,4-dihydrocinnolin-4(1H)-ones bearing diverse substituents at the C-3 quaternary sp^3 or spirocyclic center. Synthesizing structural series possessing electron-donating, electron-withdrawing, or heterocyclic moieties at C-3 has conventionally required fragmented, non-modular protocols [31–33]. While push–pull heterocyclic chromophores and azo dyes have been investigated for ICT modulation and large Stokes shifts [34–37], the lack of an efficient divergent platform for 3,4-dihydrocinnolin-4(1H)-ones has hindered systematic exploration into how C-3 electronic modulation and tautomeric S(6) chelate dynamics govern their fundamental photophysical and dual-luminescence properties [33,36].

To address these limitations, the present work introduces a convergent, metal-free, and atom-economical methodology anchored on the single bifunctional diazo linchpin (E)-2-((1-cyano-2-ethoxy-2-oxoethyl)diazenyl)benzoic acid (1). In contrast to prior multi-step or metal-catalyzed cinnoline syntheses [27–32,36], precursor 1—readily prepared in 84% yield via diazotization of anthranilic acid and Japp–Klingemann coupling with ethyl cyanoacetate—integrates an electrophilic ortho-carboxylic acid center adjacent to an active diazenyl-hydrazone linkage. Under mild, base-catalyzed conditions (triethylamine in refluxing alcohol or DMF), linchpin 1 undergoes one-pot tandem cyclocondensation with ten structurally distinct active methylene and amine synthons to deliver functionalized 3,4-dihydrocinnolin-4(1H)-ones (2–10) and the spirocyclic framework 11 in 64–85% isolated yields. Beyond synthetic modularity, this study establishes a direct correlation between C-3 substituent electronics/sterics, intramolecular resonance-assisted hydrogen bonding (RAHB) within a quasi-aromatic S(6) chelate ring (δ 15.22–16.69 ppm), and dual-emission ESIPT/TICT photophysics with massive Stokes shifts up to 143.5 nm.

2. Experimental Section

2.1. Materials, Instrumentation, and Analytical Setup

All chemical reagents, starting precursors, active methylene synthons, and spectroscopic-grade solvents were obtained from commercial vendors (Sigma-Aldrich, Alfa Aesar, and Merck) at analytical purity and utilized without additional purification. Melting points were determined in open glass capillary tubes using a Gallenkamp melting point apparatus and are uncorrected. Fourier-transform infrared (FT-IR) spectra were recorded on a Pye-Unicam SP-3-300 spectrophotometer across 4000–400 cm^{-1} using pressed potassium bromide (KBr) discs. 1H-NMR (500 MHz) and 13C-NMR (125 MHz) spectra were acquired on a JEOL ECA-500 spectrometer at 298 K in deuterated dimethyl sulfoxide (DMSO-d6), with tetramethylsilane (TMS) as internal standard. Chemical shifts (δ) are expressed in parts per million (ppm) relative to residual solvent signals, and spin-spin coupling constants (J) are reported in hertz (Hz). Peak multiplicities are designated as: s (singlet), d (doublet), t (triplet), q (quartet), m (multiplet), and br s (broad singlet). Electron ionization mass spectra (EI-MS) were recorded on a Shimadzu GC–MS–QP 1000X spectrometer at an ionizing potential of 70 eV. Elemental microanalyses (C, H, N, S, Cl) were conducted on a Perkin-Elmer 2400 Series II CHNS/O analyzer; all values were within ±0.40% of theoretical calculations. Reaction progression and compound purity were monitored by thin-layer chromatography (TLC) on Merck silica gel 60 F254 aluminum sheets, with detection under 254/365 nm UV illumination.

2.2. Synthesis of the Bifunctional Diazo Linchpin (1)

Anthranilic acid (1.37 g, 10.0 mmol) was dissolved in a stirred mixture of concentrated hydrochloric acid (5.0 mL) and distilled water (10.0 mL), and the resulting solution was chilled to 0–5 °C in an ice-water bath. An aqueous solution of sodium nitrite (0.69 g, 10.0 mmol in 10.0 mL H2O) was added dropwise over 15 min,

maintaining the internal temperature below 5 °C. The freshly prepared diazonium salt solution was then introduced slowly with vigorous stirring into an ice-cold solution containing ethyl cyanoacetate (1.13 g, 10.0 mmol) and sodium acetate trihydrate (3.0 g) in absolute ethanol (30.0 mL). The mixture was stirred at 0–5 °C for 2 h and then allowed to warm to room temperature over 1 h. The resulting bright yellow precipitate was collected by vacuum filtration, washed thoroughly with chilled water, dried in vacuo, and recrystallized from hot absolute ethanol to afford pure (E)-2-((1-cyano-2-ethoxy-2-oxoethyl)diazenyl)benzoic acid (1).

Analytical Data for 1: Yield: 84%; yellow needles; m.p. 209–211 °C (EtOH); FT-IR (KBr, ν /cm⁻¹): 3167 (br, OH/NH), 3062 (Ar C–H), 2986, 2933, 2854 (aliph C–H), 2674, 2587, 2538 (COOH dimer O–H), 2206 (C≡N), 1737 (ester C=O), 1669 (COOH C=O / C=N), 1607, 1588, 1531 (Ar C=C, N=N), 1451, 1416, 1371, 1318, 1278, 1232, 1165, 1122 (C–O, C–N), 1018, 905, 846, 810, 758 (ortho-disubstituted Ar C–H), 704, 660, 580, 518; 1H-NMR (500 MHz, DMSO-d6) δ (ppm): 13.05 (br s, 1H, COOH / hydrazone NH), 7.97 (d, J = 7.6 Hz, 1H, Ar-H ortho to COOH), 7.68 (m, 2H, Ar-H), 7.22 (t, J = 7.6 Hz, 1H, Ar-H), 4.29 (q, J = 7.1 Hz, 2H, –OCH_2CH_3), 1.28 (t, J = 7.1 Hz, 3H, –OCH_2CH_3); EI-MS (70 eV): m/z (%) = 261.07 $[M]^+$ (100%); Anal. Calcd for $C_{12}H_{11}N_3O_4$ (261.24): C, 55.17; H, 4.24; N, 16.09. Found: C, 55.17; H, 4.24; N, 16.09.

2.3. General Synthetic Procedure for 3,4-Dihydrocinnolin-4(1H)-ones (2–11)

A mixture of linchpin 1 (2.61 g, 10.0 mmol) and the appropriate active methylene synthon or nucleophilic amine (10.0 mmol)-specifically cyanoacetohydrazide (0.99 g, for 2), cyanoacetamide (0.84 g, for 3), benzylamine (1.07 g, for 4), 1-chlorobutan-2-one (1.07 g, for 5), ethyl cyanoacetate (1.13 g, for 6), diethyl malonate (1.60 g, for 7), acetylacetone (1.00 g, for 8), 2-(benzo[d]thiazol-2-yl)acetonitrile (1.74 g, for 9), 3-(2-cyanoacetyl)phenol (1.61 g, for 10), or 5-methyl-2-phenyl-2,4-dihydro-3H-pyrazol-3-one (1.74 g, for 11)—was dissolved in 30.0 mL of the specified anhydrous solvent (absolute ethanol for 2 and 3; n-butanol for 4–6 and 8–11; N,N-dimethylformamide for 7) containing triethylamine (TEA, 0.50 mL, 3.6 mmol) as a basic catalyst. Each reaction mixture was heated under gentle reflux for 8 h while monitoring completion by TLC (ethyl acetate/n-hexane). Upon complete consumption of 1, the mixture was cooled to room temperature. The resulting precipitate was collected by suction filtration, washed with cold ethanol and distilled water, dried under reduced pressure, and recrystallized from the corresponding solvent to afford analytically pure targets 2–11 in isolated yields of 64–85%.

Ethyl 2-cyano-2-(3-cyano-3-(hydrazinecarbonyl)-4-oxo-3,4-dihydrocinnolin-2(1H)-yl)acetate (2, R-501)

Yield: 76% (2.60 g); dark yellow powder; m.p. 280 °C (EtOH); FT-IR (KBr, ν /cm⁻¹): 3456 (asym NH_2/NH), 3159 (sym NH), 3059 (Ar C–H), 2989, 2881, 2812 (aliph C–H), 2214 (C≡N), 1736 (ester C=O), 1697 (lactam/hydrazide C=O), 1597, 1500 (Ar C=C, NH bend), 1377, 1308, 1273, 1219, 1176, 1119 (C–O, C–N), 1014, 964, 841, 752; ^{1}H-NMR (500 MHz, DMSO-d_6) δ (ppm): 16.68 (s, 0.71H, enolic OH / N(1)–H chelate), 16.39 (s, 0.29H, NH tautomer), 7.91 (d, J = 7.7 Hz, 1H, Ar-H5), 7.57 (t, J = 7.6 Hz, 1H, Ar-H7), 7.43 (t, J = 7.5 Hz, 1H, Ar-H6), 7.04 (d, J = 7.8 Hz, 1H, Ar-H8), 5.86 (s, 1H, –CH(CN)), 4.19 (q, J = 7.1 Hz, 2H, –OCH_2CH_3), 1.23 (t, J = 7.1 Hz, 3H, –OCH_2CH_3); EI-MS (70 eV): m/z = 342.11 $[M]^+$; UV-Vis (EtOH): λabs = 265.0 nm (A = 0.500), 395.0 nm (A = 1.634); Fluorescence (EtOH, λex = 395 nm): λem1 = 475.8 nm (2440 counts), λem2 = 533.0 nm (1438 counts); Stokes shifts: Δλ1 = 80.8 nm (4299 cm⁻¹), Δλ2 = 138.0 nm (6555 cm⁻¹); Anal. Calcd for $C_{15}H_{14}N_6O_4$ (342.31): C, 52.63; H, 4.12; N, 24.55. Found: C, 52.63; H, 4.12; N, 24.55.

Ethyl 2-(3-carbamoyl-3-cyano-4-oxo-3,4-dihydrocinnolin-2(1H)-yl)-2-cyanoacetate (3, R-502)

Yield: 78% (2.55 g); yellow crystals; m.p. 270 °C (EtOH); FT-IR (KBr, ν /cm⁻¹): 3410 (NH_2 amide), 3201 (NH), 3059 (Ar C–H), 2989, 2881, 2816 (aliph C–H), 2268, 2214 (C≡N), 1739 (ester C=O), 1697 (amide/lactam C=O), 1597, 1500 (Ar C=C, NH bend), 1377, 1308, 1273, 1219, 1176, 1119 (C–O, C–N), 1014, 841, 752; ^{1}H-NMR (500 MHz, DMSO-d_6) δ (ppm): 16.64 (s, 0.77H, enolic OH / N(1)–H chelate), 16.26 (s, 0.23H, NH tautomer), 7.91 (d, J = 7.7 Hz, 1H, Ar-H5), 7.58 (t, J = 7.6 Hz, 1H, Ar-H7), 7.43 (t, J = 7.5 Hz, 1H, Ar-H6), 7.04 (d, J = 7.8 Hz, 1H, Ar-H8), 4.20 (q, J = 7.1 Hz, 2H, –OCH_2CH_3), 3.59, 3.45 (2 × br s, 2H, –$CONH_2$), 1.24 (t, J = 7.1 Hz, 3H, –OCH_2CH_3); ^{13}C-NMR (125 MHz, DMSO-d_6) δ (ppm): 169.42 (ester C=O), 163.63 (amide C=O), 150.37 (lactam C=O / C-Ar), 133.12, 132.14, 131.97, 131.69 (Ar C–H), 124.55, 123.31, 120.92 (Ar C), 114.99, 114.39 (2 × C≡N), 102.37 (C-3 quaternary), 61.88 (–OCH_2CH_3), 60.51 (C-α), 14.98, 14.62 (–CH_3); EI-MS (70 eV): m/z = 327.10 $[M]^+$; UV-Vis (EtOH): λabs = 265.0 nm (A = 0.126), 395.0 nm (A = 0.539); Fluorescence (EtOH, λex = 395 nm): λem = 469.8 nm (6086 counts); Stokes shift: Δλ = 74.8 nm (4031 cm⁻¹); Anal. Calcd for $C_{15}H_{13}N_5O_4$ (327.30): C, 55.05; H, 4.00; N, 21.40. Found: C, 55.05; H, 4.00; N, 21.40.

Ethyl 2-(3-amino-4-oxo-3-phenyl-3,4-dihydrocinnolin-2(1H)-yl)-2-cyanoacetate (4)
Yield: 68% (2.38 g); yellow crystals; m.p. 242 °C (BuOH); FT-IR (KBr, ν /cm⁻¹): 3429 (NH_2), 3059, 3032 (Ar C–H), 2962, 2873, 2831 (aliph C–H), 2210 (C≡N), 1739 (ester C=O), 1697 (lactam C=O), 1597, 1496 (Ar C=C, NH bend), 1377, 1308, 1273, 1215, 1169, 1146, 1119 (C–O, C–N), 1022, 957, 833, 752, 698 (Ar C–H); ^{1}H-NMR (500 MHz, DMSO-d_6) δ (ppm): 7.93 (d, J = 7.7 Hz, 1H, Ar-H5), 7.58 (t, J = 7.6 Hz, 1H, Ar-H7), 7.41–7.44 (m, 4H, cinnoline H-6 and phenyl Ar-H), 7.11–7.20 (m, 2H, phenyl Ar-H), 7.04 (d, J = 7.8 Hz, 1H, Ar-H8), 4.15 (q, J = 7.1 Hz, 2H, –OCH_2CH_3), 3.47 (br s, 2H, NH_2), 1.23 (t, J = 7.1 Hz, 3H, –OCH_2CH_3); ^{13}C-NMR (125 MHz, DMSO-d_6) δ (ppm): 169.57 (ester C=O), 163.59 (lactam C=O), 150.10 (Ar C), 133.02, 132.24, 131.72 (Ar C–H), 128.88, 128.73, 128.13, 127.70 (phenyl C–H), 124.54, 123.32, 121.11 (Ar C), 114.93 (C≡N), 102.40 (C-α), 65.47 (C-3 sp^3 C–NH_2), 64.26 (–OCH_2CH_3), 14.12 (–CH_3); EI-MS (70 eV): m/z = 350.14 $[M]^+$; Anal. Calcd for $C_{19}H_{18}N_4O_3$ (350.38): C, 65.13; H, 5.18; N, 15.99. Found: C, 65.13; H, 5.18; N, 15.99.

Ethyl 2-(3-chloro-4-oxo-3-propionyl-3,4-dihydrocinnolin-2(1H)-yl)-2-cyanoacetate (5, R-504)
Yield: 64% (2.24 g); light yellow crystals; m.p. 138 °C (BuOH); FT-IR (KBr, ν /cm⁻¹): 3437 (NH), 3143 (NH), 2989, 2881, 2692 (aliph C–H), 2225 (C≡N), 1751 (ester/propionyl C=O), 1697 (lactam C=O), 1589, 1508 (Ar C=C), 1419, 1381, 1311, 1281, 1223, 1176, 1146, 1099 (C–O, C–N), 1022, 810, 760 (C–Cl, Ar C–H); ^{1}H-NMR (500 MHz, DMSO-d_6) δ (ppm): 16.40 (s, 0.45H, enolic OH / N(1)–H chelate), 14.39 (s, 0.35H, NH tautomer), 11.78 (s, 0.20H, NH/OH), 8.04 (d, J = 7.7 Hz, 1H, Ar-H5), 7.30–7.82 (m, 3H, Ar-H6, H7, H8), 4.91–4.96 (m, 1H, –CH(CN)), 4.29 (q, J = 7.1 Hz, 2H, –OCH_2CH_3), 1.27 (t, J = 7.1 Hz, 3H, ester –CH_3), 1.19 (t, J = 7.2 Hz, 3H, propionyl –CH_3); ^{13}C-NMR (125 MHz, DMSO-d_6) δ (ppm): 169.11 (ester C=O), 167.91 (propionyl C=O), 166.08 (lactam C=O), 160.39, 143.25, 136.23 (Ar C), 133.40, 131.64, 125.19, 123.26 (Ar C–H), 115.98 (C≡N), 115.10, 114.39 (Ar C), 108.44 (C-3 quaternary C–Cl), 62.84, 62.14, 61.65, 60.44 (–OCH_2– and propionyl –CH_2–), 14.99, 14.61, 14.52, 14.40 (–CH_3); EI-MS (70 eV): m/z = 349.08 $[M]^+$, 351.08 $[M+2]^+$ (3:1 isotopic ratio); UV-Vis (EtOH): λabs = 265.0 nm (A = 0.740), 365.1 nm (A = 1.922), 380.0 nm (sh, A = 1.863); Fluorescence (EtOH, λex = 365 nm): λem1 = 469.4 nm (3372 counts), λem2 = 508.6 nm (2089 counts); Stokes shifts: Δλ1 = 104.3 nm (6086 cm⁻¹), Δλ2 = 143.5 nm (7728 cm⁻¹); Anal. Calcd for $C_{16}H_{16}ClN_3O_4$ (349.77): C, 54.94; H, 4.61; Cl, 10.14; N, 12.01. Found: C, 54.94; H, 4.61; Cl, 10.14; N, 12.01.

Ethyl 3-cyano-2-(1-cyano-2-ethoxy-2-oxoethyl)-4-oxo-1,2,3,4-tetrahydrocinnoline-3-carboxylate (6)
Yield: 72% (2.57 g); yellow crystals; m.p. 278 °C (BuOH); FT-IR (KBr, ν /cm⁻¹): 3437 (NH), 3074 (Ar C–H), 2997, 2881, 2785 (aliph C–H), 2218 (C≡N), 1817 (ester C=O), 1697 (lactam/ester C=O), 1597, 1493 (Ar C=C), 1373, 1308, 1273, 1219, 1176, 1119 (C–O, C–N), 1014, 841, 752; ^{1}H-NMR (500 MHz, DMSO-d_6) δ (ppm): 16.60 (s, 0.85H, enolic OH / N(1)–H chelate), 15.82 (s, 0.15H, NH/enol), 7.91 (d, J = 7.7 Hz, 1H, Ar-H5), 7.58 (t, J = 7.6 Hz, 1H, Ar-H7), 7.04–7.44 (m, 2H, Ar-H6, Ar-H8), 4.18 (q, J = 7.1 Hz, 4H, 2 × –OCH_2CH_3), 3.60 (s, 1H, –CH(CN)COOEt), 1.22–1.28 (m, 6H, 2 × –OCH_2CH_3); ^{13}C-NMR (125 MHz, DMSO-d_6) δ (ppm): 169.24 (ester C=O), 163.73 (ester C=O), 160.02 (lactam C=O), 150.81, 143.95 (Ar C), 133.23, 132.02, 131.66 (Ar C–H), 124.23, 123.25, 120.64 (Ar C), 115.14, 115.05 (2 × C≡N), 102.28 (C-3 quaternary / C-α), 61.90, 60.43 (2 × –OCH_2CH_3), 30.74 (aliphatic C), 14.99 (–CH_3); EI-MS (70 eV): m/z = 356.11 $[M]^+$; Anal. Calcd for $C_{17}H_{16}N_4O_5$ (356.34): C, 57.30; H, 4.53; N, 15.72. Found: C, 57.30; H, 4.53; N, 15.72.

Ethyl 2-(1-cyano-2-ethoxy-2-oxoethyl)-4-oxo-1,2,3,4-tetrahydrocinnoline-3-carboxylate (7, R-506)
Yield: 77% (2.55 g); yellow crystals; m.p. 280 °C (DMF); FT-IR (KBr, ν /cm⁻¹): 3437 (NH), 3062 (Ar C–H), 2993, 2881, 2781 (aliph C–H), 2222 (C≡N), 1813 (ester C=O), 1693 (lactam/ester C=O), 1597, 1500 (Ar C=C), 1377, 1308, 1277, 1219, 1176, 1119 (C–O, C–N), 1014, 957, 837, 756; ^{1}H-NMR (500 MHz, DMSO-d_6) δ (ppm): 16.50 (s, 1H, enolic OH / N(1)–H chelate), 7.91 (d, J = 7.7 Hz, 1H, Ar-H5), 7.57 (t, J = 7.6 Hz, 1H, Ar-H7), 7.43 (t, J = 7.5 Hz, 1H, Ar-H6), 7.04 (d, J = 7.8 Hz, 1H, Ar-H8), 4.18 (q, J = 7.1 Hz, 4H, overlapping 2 × –OCH_2CH_3), 1.23 (t, J = 7.1 Hz, 6H, overlapping 2 × –OCH_2CH_3); EI-MS (70 eV): m/z = 331.12 $[M]^+$; UV-Vis (EtOH): λabs = 265.0 nm (A = 0.366), 389.9 nm (A = 1.132); Fluorescence (EtOH, λex = 390 nm): λem = 474.0 nm (5873 counts); Stokes shift: Δλ = 84.1 nm (4550 cm⁻¹); Anal. Calcd for $C_{16}H_{17}N_3O_5$ (331.33): C, 58.00; H, 5.17; N, 12.68. Found: C, 58.00; H, 5.17; N, 12.68.

Ethyl 2-(3-acetyl-4-oxo-3,4-dihydrocinnolin-2(1H)-yl)-2-cyanoacetate (8, R-507)
Yield: 85% (2.56 g); dark yellow crystals; m.p. 274 °C (BuOH); FT-IR (KBr, ν /cm⁻¹): 3498 (NH), 3062 (Ar C–H), 2985, 2881, 2819 (aliph C–H), 2225 (C≡N), 1693 (br, ester/acetyl/lactam C=O), 1597, 1500 (Ar C=C), 1377, 1311, 1277, 1223, 1176, 1119 (C–O, C–N), 1014, 960, 837, 756; ^{1}H-NMR (500 MHz, DMSO-d_6) δ (ppm): 16.51 (s, 0.85H, enolic OH / N(1)–H chelate), 15.59 (s, 0.15H, NH/enol), 7.91 (d, J = 7.7 Hz, 1H, Ar-H5), 7.58 (t, J = 7.6 Hz, 1H, Ar-H7), 7.44 (t, J = 7.5 Hz, 1H, Ar-H6), 7.04 (d, J = 7.8 Hz, 1H, Ar-H8), 4.20 (q, J

= 7.1 Hz, 2H, –OCH_2CH_3), 3.04 (s, 3H, –$COCH_3$), 1.24 (t, J = 7.1 Hz, 3H, –OCH_2CH_3); ^{13}C-NMR (125 MHz, DMSO-d_6) δ (ppm): 169.46 (ester C=O), 169.37 (acetyl C=O), 163.57 (lactam C=O), 160.10, 150.31, 143.47 (Ar C), 133.23, 132.03, 131.69 (Ar C–H), 124.70, 123.32, 120.64 (Ar C), 115.04, 114.93 (C≡N), 105.48 (C-3 quaternary), 102.54 (C-α), 62.15, 60.54 (–OCH_2CH_3), 14.97, 14.56 (–$COCH_3$ & –CH_3); EI-MS (70 eV): m/z = 301.11 $[M]^+$; UV-Vis (EtOH): λabs = 265.0 nm (A = 0.401), 395.0 nm (A = 1.258); Fluorescence (EtOH, λex = 395 nm): λem = 486.6 nm (8516 counts); Stokes shift: Δλ = 91.6 nm (4766 cm^{-1}); Anal. Calcd for $C_{15}H_{15}N_3O_4$ (301.30): C, 59.80; H, 5.02; N, 13.95. Found: C, 59.80; H, 5.02; N, 13.95.

Ethyl 2-(3-(benzo[d]thiazol-2-yl)-3-cyano-4-oxo-3,4-dihydrocinnolin-2(1H)-yl)-2-cyanoacetate (9, R-508)
Yield: 80% (3.34 g); dark yellow crystals; m.p. 240 °C (BuOH); FT-IR (KBr, ν /cm^{-1}): 3433, 3313, 3275 (NH), 3074 (Ar C–H), 2997, 2881, 2792 (aliph C–H), 2276, 2225 (C≡N), 1689 (ester/lactam C=O), 1597, 1500 (Ar C=C, benzothiazole C=N), 1377, 1311, 1281, 1219, 1180, 1115 (C–O, C–N), 1014, 937, 841, 756 (C–S, Ar C–H); ^{1}H-NMR (500 MHz, DMSO-d_6) δ (ppm): 16.32 (s, 0.80H, enolic OH / N(1)–H chelate), 15.22 (s, 0.20H, NH/enol), 9.63 (s, 1H, NH), 7.91 (d, J = 7.7 Hz, 1H, Ar-H5), 7.57–7.58 (m, 2H, cinnoline H-7 & benzothiazole Ar-H), 7.45 (t, J = 7.5 Hz, 1H, Ar-H6), 7.05 (d, J = 7.8 Hz, 1H, Ar-H8), 6.73–6.94 (m, 2H, benzothiazole Ar-H), 4.20 (q, J = 7.1 Hz, 2H, –OCH_2CH_3), 1.24 (t, J = 7.1 Hz, 3H, –OCH_2CH_3); ^{13}C-NMR (125 MHz, DMSO-d_6) δ (ppm): 169.38 (ester C=O), 163.41 (lactam C=O), 161.47 (benzothiazole C=N), 149.97, 148.58 (Ar C), 133.36, 131.98, 131.69 (Ar C–H), 125.59, 123.39, 120.35, 119.31 (benzothiazole Ar C–H), 115.07, 114.74 (2 × C≡N), 102.83 (C-3 quaternary / C-α), 62.32, 60.64 (–OCH_2CH_3), 26.84 (aliphatic C), 14.95, 14.53 (–CH_3); EI-MS (70 eV): m/z = 417.09 $[M]^+$; UV-Vis (EtOH): λabs = 265.0 nm (A = 0.744), 365.1 nm (A = 1.720), 395.0 nm (A = 1.955); Fluorescence (EtOH, λex = 395 nm): λem1 = 479.6 nm (7078 counts), λem2 = 521.6 nm (4807 counts); Stokes shifts: Δλ1 = 84.6 nm (4466 cm^{-1}), Δλ2 = 126.6 nm (6145 cm^{-1}); Anal. Calcd for $C_{21}H_{15}N_5O_3S$ (417.44): C, 60.42; H, 3.62; N, 16.78; S, 7.68. Found: C, 60.42; H, 3.62; N, 16.78; S, 7.68.

Ethyl 2-cyano-2-(3-cyano-3-(3-hydroxybenzoyl)-4-oxo-3,4-dihydrocinnolin-2(1H)-yl)acetate (10, R-509)
Yield: 71% (2.87 g); yellow crystals; m.p. 282 °C (BuOH); FT-IR (KBr, ν /cm^{-1}): 3483 (phenolic O–H / NH), 3062 (Ar C–H), 2989, 2881, 2816 (aliph C–H), 2222 (C≡N), 1697 (br, ester/benzoyl/lactam C=O), 1597, 1496 (Ar C=C), 1377, 1308, 1277, 1219, 1176, 1149, 1119 (C–O, C–N), 1014, 960, 841, 756; ^{1}H-NMR (500 MHz, DMSO-d_6) δ (ppm): 16.54 (s, 0.88H, enolic OH / N(1)–H chelate), 15.66 (s, 0.12H, NH/enol), 7.91 (d, J = 7.7 Hz, 1H, Ar-H5), 7.57–7.58 (m, 3H, cinnoline & benzoyl Ar-H), 7.44 (m, 2H, Ar-H), 7.04–7.06 (m, 2H, Ar-H), 4.19 (q, J = 7.1 Hz, 2H, –OCH_2CH_3), 3.80 (br s, 1H, phenolic OH), 1.24 (t, J = 7.1 Hz, 3H, –OCH_2CH_3); ^{13}C-NMR (125 MHz, DMSO-d_6) δ (ppm): 169.33 (ester C=O), 163.61 (lactam C=O), 160.26 (phenolic C–OH), 150.45 (Ar C cinnoline), 143.70 (benzoyl C-ipso), 133.23, 132.04, 131.68 (Ar C–H), 124.69, 123.31, 120.64 (Ar C and C–H), 115.03, 114.84 (2 × C≡N), 102.45 (C-α), 64.34 (C-3 quaternary), 62.11, 60.51 (–OCH_2CH_3), 14.98, 14.57 (–CH_3); EI-MS (70 eV): m/z = 404.11 $[M]^+$; UV-Vis (EtOH): λabs = 265.0 nm (A = 0.604), 395.0 nm (A = 1.890); Fluorescence (EtOH, λex = 395 nm): λem = 467.0 nm (4714 counts); Stokes shift: Δλ = 72.0 nm (3903 cm^{-1}); Anal. Calcd for $C_{21}H_{16}N_4O_5$ (404.38): C, 62.37; H, 3.99; N, 13.86. Found: C, 62.37; H, 3.99; N, 13.86.

Ethyl 2-cyano-2-(3'-methyl-4,5'-dioxo-1'-phenyl-1,1',4,5'-tetrahydro-2H-spiro[cinnoline-3,4'-pyrazol]-2-yl)acetate (11)
Yield: 66% (2.75 g); yellow crystals; m.p. 268 °C (BuOH); FT-IR (KBr, ν /cm^{-1}): 3487 (NH), 2962, 2873 (aliph C–H), 2206 (C≡N), 1743 (pyrazolone/ester C=O), 1701 (lactam C=O), 1597, 1504 (Ar C=C, pyrazole C=N), 1377, 1308, 1273, 1215, 1169, 1119 (C–O, C–N), 1018, 953, 833, 752, 698; ^{1}H-NMR (500 MHz, DMSO-d_6) δ (ppm): 16.69 (s, 0.82H, enolic OH / N(1)–H chelate), 16.44 (s, 0.18H, NH tautomer), 7.91 (d, J = 7.7 Hz, 1H, Ar-H5), 7.57 (t, J = 7.6 Hz, 1H, Ar-H7), 7.43 (t, J = 7.5 Hz, 1H, Ar-H6), 7.03 (d, J = 7.8 Hz, 1H, Ar-H8), 4.14 (q, J = 7.1 Hz, 2H, –OCH_2CH_3), 1.59 (s, 3H, pyrazolone C3'–CH_3), 0.89 (t, J = 7.1 Hz, 3H, ester –CH_3); EI-MS (70 eV): m/z = 417.14 $[M]^+$; Anal. Calcd for $C_{22}H_{19}N_5O_4$ (417.42): C, 63.30; H, 4.59; N, 16.78. Found: C, 63.30; H, 4.59; N, 16.78.

2.4. Optical and Photophysical Measurement Protocols

To probe the impact of C-3 electronic and steric modulation while avoiding redundant non-conjugated or sterically congested analogues (4, 6, and 11), seven representative fluorophores—namely compounds 2 (R-501), 3 (R-502), 5 (R-504), 7 (R-506), 8 (R-507), 9 (R-508), and 10 (R-509)—were selected for steady-state UV-Vis absorption and fluorescence emission measurements in spectroscopic-grade absolute ethanol at 298 K. Electronic absorption profiles were collected across 200–900 nm on a double-beam UV-Vis spectrophotometer using matched 1.0 cm quartz cuvettes. Steady-state photoluminescence emission spectra were recorded on a

calibrated spectrofluorometer over 400–900 nm upon selective photoexcitation at the corresponding ICT absorption maxima (λex = 365–395 nm), utilizing 5.0 nm excitation and emission slit widths. Stokes shifts were calculated in both wavelength (Δλ = λem − λabs, nm) and wavenumber (Δν = (1/λabs − 1/λem) × 10^7, cm^{-1}) units.

3. Results and Discussion

3.1. Synthetic Chemistry Rationalization and Divergent Annulation Cascades

The construction of polyfunctionalized 3,4-dihydrocinnolin-4(1H)-ones was accomplished through a divergent cascade strategy anchored on the bifunctional diazo building block (E)-2-((1-cyano-2-ethoxy-2-oxoethyl)diazenyl)benzoic acid (1). Synthesized in 84% yield via aqueous diazotization of anthranilic acid followed by buffered Japp–Klingemann coupling with ethyl cyanoacetate, linchpin 1 combines two mutually reactive vectors: an electrophilic ortho-carboxylic acid center and an activated diazenyl-hydrazone motif. Upon exposure to catalytic triethylamine in refluxing alcohol, precursor 1 undergoes facile tandem cyclocondensation sequences with varied active methylene synthons and primary amine nucleophiles (Schemes 1 and 2).

As shown in Scheme 1, condensation of linchpin 1 with active methylene precursors and nucleophiles—specifically cyanoacetohydrazide, cyanoacetamide, benzylamine, 1-chlorobutan-2-one, and ethyl cyanoacetate—proceeds through initial carbanion attack on the electrophilic diazenyl/hydrazone carbon. The adjacent ortho-carboxylic group undergoes subsequent intramolecular nucleophilic acyl substitution, driving ring closure accompanied by the elimination of water or ethanol. This tandem sequence establishes the functionalized 3,4-dihydrocinnoline core in good to high isolated yields (64–78%): 2 (76%), 3 (78%), 4 (68%), 5 (64%), and 6 (72%).

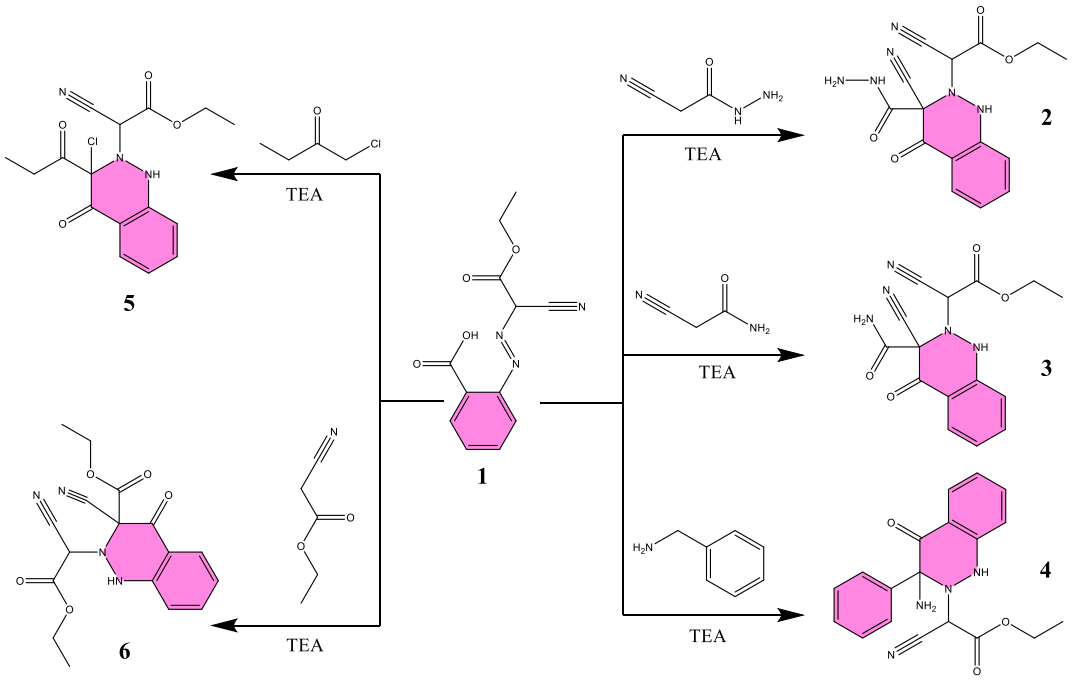

Scheme 1. Convergent base-catalyzed synthesis of functionalized 3,4-dihydrocinnolin-4(1H)-one derivatives (2–6) from bifunctional diazo linchpin 1 (TEA, EtOH or n-BuOH, reflux, 8 h).

Under identical catalytic conditions, divergent annulations of precursor 1 with symmetric and unsymmetric bis-electrophilic/bifunctional nucleophiles—diethyl malonate, acetylacetone, 2-(benzo[d]thiazol-2-yl)acetonitrile, 3-(2-cyanoacetyl)phenol, and 5-methyl-2-phenyl-2,4-dihydro-3H-pyrazol-3-one—afforded specialized cinnolinones 7–10 and the unique spirocyclic adduct 11 (Scheme 2). Isolated yields across this series reflect the electronic nature and steric requirements of the nucleophilic synthons: diethyl malonate cleanly gave 7 in 77% yield; highly reactive acetylacetone produced the 3-acetyl derivative 8 in an outstanding 85% yield; 2-(benzo[d]thiazol-2-yl)acetonitrile furnished the benzothiazole-appended fluorophore 9 in 80% yield; 3-(2-cyanoacetyl)phenol provided 10 in 71% yield; and pyrazolone delivered the sterically congested spiro[cinnoline-3,4'-pyrazole] derivative 11 in 66% yield. Regiochemical fidelity across these transformations is

governed by preferential nucleophilic addition to the diazenyl carbon followed by intramolecular cyclization onto the ortho-carboxylic group.

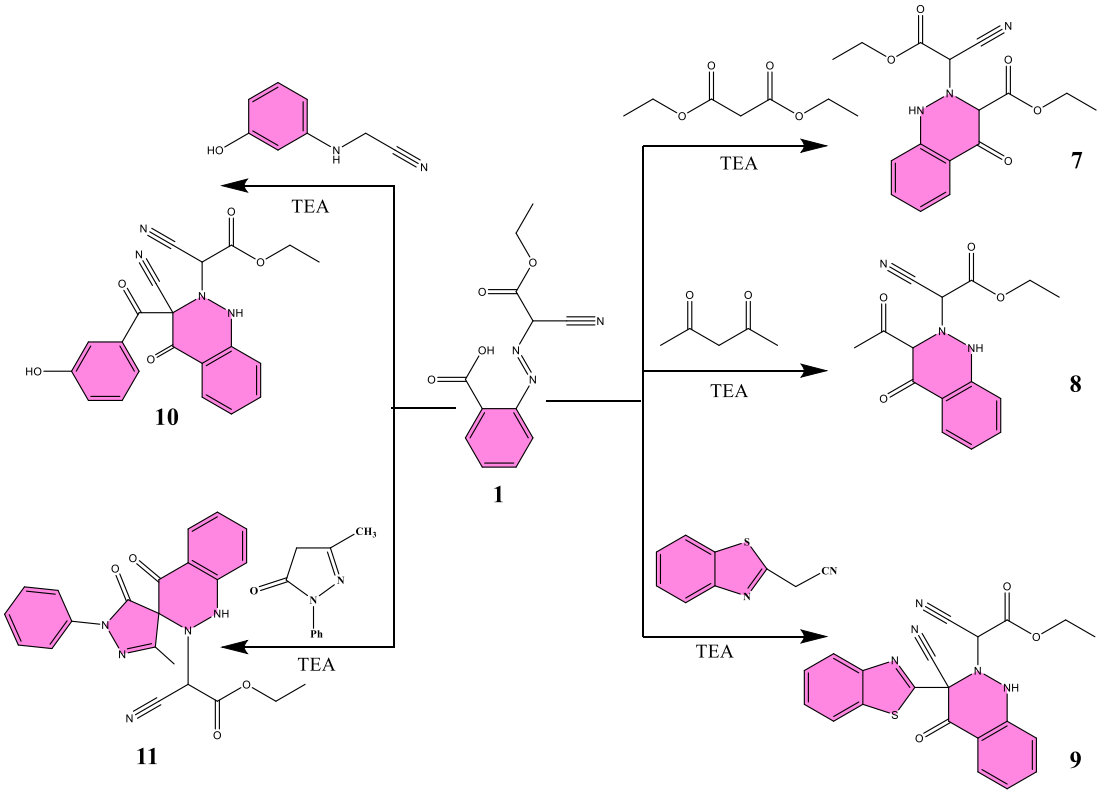

Scheme 2. Divergent synthesis of functionalized 3,4-dihydrocinnolin-4(1H)-ones (7–10) and spiro[cinnoline-3,4'-pyrazole] adduct 11 from linchpin 1 (TEA, n-BuOH or DMF, reflux, 8 h).

Table 1. Summary of reaction conditions, isolated yields, melting points, and molecular formulas for compounds 1–11 (see Table S1 in Supplementary Materials for chemical structures and exact masses).

Comp. No.	Dye Code	C-3 Substituent Motif	UV-Vis λabs (nm) [Absorbance, A]	Fluorescence λem (nm) [Intensity, counts]	Stokes Shift Δλ (nm) [Δν, cm^{-1}]
2	R-501	–CONHNH₂ / –CN	265.0 [0.500], 395.0 [1.634]	475.8 [2440], 533.0 [1438]	80.8 [4299] (138.0 [6555])
3	R-502	–CONH₂ / –CN	265.0 [0.126], 395.0 [0.539]	469.8 [6086]	74.8 [4031]
5	R-504	–COCH₂CH₃ / –Cl	265.0 [0.740], 365.1 [1.922], 380.0 (sh) [1.863]	469.4 [3372], 508.6 [2089]	104.3 [6086] (143.5 [7728])
7	R-506	–COOEt / –H	265.0 [0.366], 389.9 [1.132]	474.0 [5873]	84.1 [4550]
8	R-507	–COCH₃ / –H	265.0 [0.401], 395.0 [1.258]	486.6 [8516]	91.6 [4766]
9	R-508	Benzothiazol-2-yl / –CN	265.0 [0.744], 365.1 [1.720], 395.0 [1.955]	479.6 [7078], 521.6 [4807]	84.6 [4466] (126.6 [6145])
10	R-509	3-HO–C₆H₄–CO– / –CN	265.0 [0.604], 395.0 [1.890]	467.0 [4714]	72.0 [3903]

Comp. No.	Dye Code	C-3 Substituent Motif	UV-Vis λabs (nm) [Absorbance, A]	Fluorescence λem (nm) [Intensity, counts]	Stokes Shift Δλ (nm) [Δν, cm^{-1}]
8 (R-507)	Acetylacetone	n-BuOH	85	274	$C_{15}H_{15}N_3O_4$ (301.11)
9 (R-508)	2-(Benzo[d]thiazol-2-yl)acetonitrile	n-BuOH	80	240	$C_{21}H_{15}N_5O_3S$ (417.09)
10 (R-509)	3-(2-Cyanoacetyl)phenol	n-BuOH	71	282	$C_{21}H_{16}N_4O_5$ (404.11)
11 (R-510)	5-Methyl-2-phenyl-2,4-dihydro-3H-pyrazol-3-one	n-BuOH	66	268	$C_{22}H_{19}N_5O_4$ (417.14)

3.2. Plausible Reaction Mechanism for Tandem Annulation Cascades

To rationalize the formation of target 3,4-dihydrocinnolin-4(1H)-ones (2–10) and the spirocyclic adduct 11, a plausible multi-step tandem cyclization pathway is outlined in Scheme 3. Precursor (E)-2-((1-cyano-2-ethoxy-2-oxoethyl)diazenyl)benzoic acid (1) exists in dynamic equilibrium between its azo form and the tautomeric hydrazone form 1'. Under basic catalysis, triethylamine (Et3N) abstracts an acidic methylene proton from the incoming synthon (R–CH2–X) to generate the resonance-stabilized carbon nucleophile $[R–CH–X]^-$.

In Step 1, this nucleophile undergoes an intermolecular conjugate addition across the electrophilic diazenyl/hydrazone linkage of precursor 1, establishing a stable carbon–nitrogen/carbon–carbon linkage to yield the acyclic intermediate [A]. In Step 2, the adjacent ortho-carboxylic acid moiety on the anthranilate ring acts as an electrophilic acceptor. The newly installed carbanionic/enolate center at C-3 executes an intramolecular nucleophilic attack onto the carboxyl carbon [C-3 → C-4(=O)OH], forming the six-membered cyclic hemiacetal/hydroxy intermediate [B]. In Step 3, base-mediated expulsion of a water molecule (–H2O) drives irreversible ring closure, locking the core into the fused 3,4-dihydrocinnolin-4(1H)-one nucleus containing a non-aromatic quaternary sp^3 carbon at C-3.

In Step 4, proton transfer and dynamic tautomerization generate the keto–enol / lactam–lactim equilibrium. The enolic/lactam proton is strongly sequestered by the adjacent carbonyl oxygen of the C-α ester or C-3 acyl group via resonance-assisted hydrogen bonding (RAHB), establishing the rigid, quasi-aromatic six-membered S(6) chelate ring. This chelation accounts for the diagnostic low-field 1H-NMR resonance at δ 15.22–16.69 ppm and sets the stage for ultrafast excited-state intramolecular proton transfer (ESIPT). In the divergent case of pyrazolone synthon (producing compound 11), nucleophilic attack occurs through the reactive C-4 position of the pyrazolin-5-one core, followed by tandem cyclocondensation onto the carboxyl group to establish the sterically congested, orthogonally oriented spiro[cinnoline-3,4'-pyrazole] architecture.

3.3. Structural Elucidation and Spectroscopic Confirmation of S(6) Chelate Tautomerism

The molecular constitutions and regiochemical integrity of compounds 1–11 were established through complementary FT-IR, 1D/2D NMR, EI-MS, and elemental analyses. The FT-IR spectrum of linchpin 1 exhibited characteristic broad absorption envelopes at 3167 cm^{-1} and 2674–2538 cm^{-1}, assignable to hydrogen-bonded carboxylic acid O–H / hydrazone N–H vibrations. A sharp absorption at 2206 cm^{-1} confirmed the nitrile (C≡N) group, while distinct carbonyl bands appeared at 1737 cm^{-1} (ester C=O) and 1669 cm^{-1} (carboxylic C=O / C=N). Upon cyclization to give 2–11, the broad carboxylic O–H envelope disappeared completely, verifying cyclization of the ortho-carboxyl group.

In the cyclized derivatives 2–11, an intense diagnostic band appeared at 1689–1700 cm^{-1}, characteristic of the cyclic lactam carbonyl (C=O) of the 3,4-dihydrocinnolin-4-one framework. Ester carbonyls resonated at 1735–1751 cm^{-1}, while cyano groups displayed sharp stretching bands at 2206–2275 cm^{-1}. Compounds 2 and 3 showed dual bands at 3409–3455 cm^{-1} for primary amino and amide/hydrazide stretching modes, whereas compound 9 showed C–S–C modes at 755 cm^{-1}, confirming benzothiazole integration.

In 1H-NMR spectra (DMSO-d6), compounds 2, 3, and 5–11 systematically displayed an extraordinary downfield singlet resonating between δ 15.22 and 16.69 ppm (e.g., δ 16.68 ppm in 2, δ 16.64 ppm in 3, δ 16.40 ppm in 5, δ 16.60 ppm in 6, δ 16.50 ppm in 7, δ 16.51 ppm in 8, δ 16.32 ppm in 9, δ 16.54 ppm in 10, and δ

16.69 ppm in 11). This extreme downfield shift reflects a dynamic keto–enol / lactam–lactim equilibrium wherein the enolic OH or ring N(1)–H proton engages in strong intramolecular resonance-assisted hydrogen bonding (RAHB) with the adjacent carbonyl oxygen, forming a stable six-membered quasi-aromatic S(6) chelate ring [20,23].

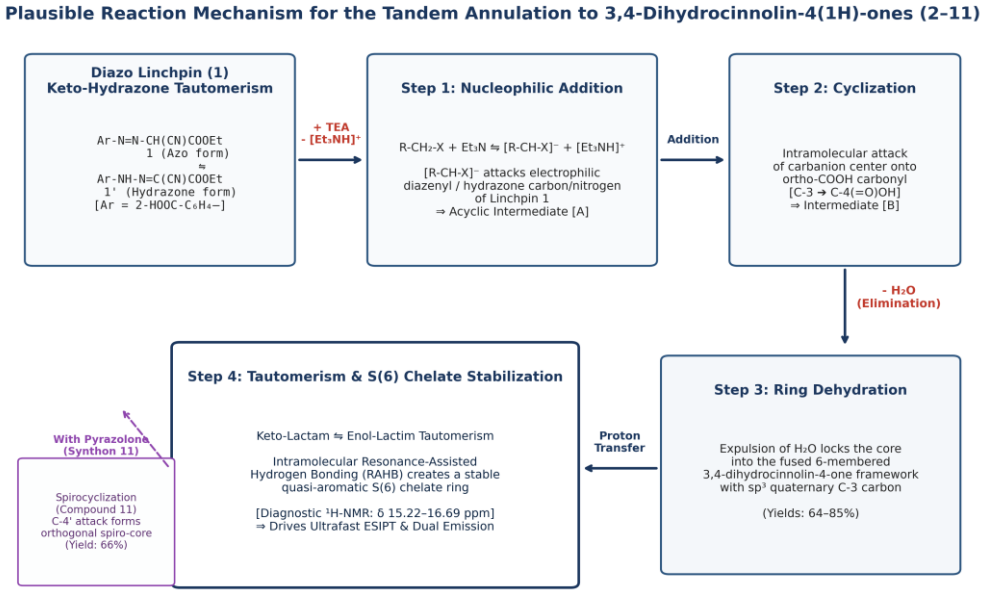

Scheme 3. Plausible stepwise tandem cyclocondensation mechanism and S(6) chelate ring stabilization in 3,4-dihydrocinnolin-4(1H)-ones (2–11).

The fused benzo-ring protons displayed consistent splitting patterns across the series: the peri-proton H-5 resonated as a doublet at δ 7.90–8.04 ppm (J = 7.7 Hz), deshielded by through-space magnetic anisotropy from the C-4 carbonyl oxygen. Conversely, H-8 appeared as an upfield doublet at δ 7.03–7.06 ppm (J = 7.8 Hz) due to shielding from the adjacent nitrogen atom. The H-6 and H-7 protons appeared as triplets/multiplets at δ 7.41–7.45 ppm and δ 7.56–7.59 ppm, respectively. In 13C-NMR spectra, the lactam carbonyl carbon (C-4) was observed at δ 160.02–166.08 ppm, while the quaternary sp³ C-3 carbon resonated at δ 64.34–108.44 ppm (δ 102.37 ppm in 3, δ 65.47 ppm in 4, δ 108.44 ppm in 5, δ 105.48 ppm in 8, and δ 102.83 ppm in 9). This chemical shift range provides definitive proof of the reduced 3,4-dihydrocinnoline state rather than a fully oxidized cinnoline system. Molecular weights were confirmed by EI-MS, with compound 5 displaying the expected 3:1 isotopic chlorine doublet at m/z 349.08 and 351.08.

3.4. Comparative Photophysical Evaluation and Spectral Characteristics

To evaluate how C-3 electronic and steric modulation governs optical behavior, the steady-state UV-Vis absorption and photoluminescence spectra of seven representative fluorophores—2 (R-501), 3 (R-502), 5 (R-504), 7 (R-506), 8 (R-507), 9 (R-508), and 10 (R-509)—were systematically investigated in absolute ethanol at 298 K (Table 2; Figures 1 and 2).

Dye Code	Comp. No.	C-3 Substituent Motif	UV-Vis Absorption λabs (nm) [Absorbance, A]	Fluorescence Emission λem (nm) [Intensity, counts]	Stokes Shift Δλ (nm)
R-501	2	–CONHNH₂ / –CN	265.0 [0.500], 395.0 [1.634]	475.8 [2440], 533.0 [1438]	80.8 (138.0)
R-502	3	–CONH₂ / –CN	265.0 [0.126], 395.0 [0.539]	469.8 [6086]	74.8

Dye Code	Comp. No.	C-3 Substituent Motif	UV-Vis Absorption λabs (nm) [Absorbance, A]	Fluorescence Emission λem (nm) [Intensity, counts]	Stokes Shift Δλ (nm)
R-504	5	–$COCH_2CH_3$ / –Cl	265.0 [0.740], 365.1 [1.922], 380.0 [1.863]	469.4 [3372], 508.6 [2089]	104.3 (143.5)
R-506	7	–COOEt / –H	265.0 [0.366], 389.9 [1.132]	474.0 [5873]	84.1
R-507	8	–$COCH_3$ / –H	265.0 [0.401], 395.0 [1.258]	486.6 [8516]	91.6
R-508	9	Benzothiazol-2-yl / –CN	265.0 [0.744], 365.1 [1.720], 395.0 [1.955]	479.6 [7078], 521.6 [4807]	84.6 (126.6)
R-509	10	3-HO–C_6H_4–CO– / –CN	265.0 [0.604], 395.0 [1.890]	467.0 [4714]	72.0

Table 2. Experimental UV-Vis electronic absorption and steady-state photoluminescence emission parameters of target 3,4-dihydrocinnolin-4(1H)-one fluorophores in absolute ethanol at 298 K.

3.4.1. Electronic Absorption (UV-Vis) and ICT Band Modulation

- All seven investigated derivatives share a sharp, high-energy absorption band centered at 265.0 nm (A = 0.126–0.744), attributable to localized π→π* transitions within the fused benzene-cinnolinone core. In addition, each compound exhibits a broad, intense low-energy intramolecular charge transfer (ICT) envelope spanning 365.1–395.0 nm (Figure 1). Compounds 2 (R-501), 3 (R-502), 8 (R-507), 9 (R-508), and 10 (R-509) display their primary ICT maxima at 395.0 nm, while the ethyl ester derivative 7 (R-506) appears slightly blue-shifted at 389.9 nm. Across this group, ICT absorbance scales with substituent conjugation and acceptor strength, peaking for benzothiazolyl derivative 9 (A = 1.955) and 3-hydroxybenzoyl analogue 10 (A = 1.890), whereas the unconjugated primary amide 3 exhibits the lowest absorbance (A = 0.539). Notably, the sterically congested C-3 chloro/propionyl derivative 5 (R-504) undergoes a pronounced 30 nm hypsochromic shift of its ICT maximum to 365.1 nm (A = 1.922, accompanied by a shoulder at 380.0 nm), reflecting steric twisting that diminishes ground-state conjugation between the C-3 acyl group and the cinnolinone chromophore.

3.4.2. Comparative Fluorescence Emission, Dual-Band (ESIPT/TICT) Dynamics, and Stokes Shifts

Selective excitation into the ICT band (λex = 365–395 nm) produces cyan-to-blue photoluminescence across 467.0–486.6 nm (Figure 2), with relative radiative intensities following the clear hierarchy: 8 (R-507, 8516 counts) > 9 (R-508, 7078 counts) > 3 (R-502, 6086 counts) > 7 (R-506, 5873 counts) > 10 (R-509, 4714 counts) > 5 (R-504, 3372 counts) > 2 (R-501, 2440 counts). This ranking directly mirrors C-3 electronic coupling and conformational rigidity. Coplanar, strongly conjugated acceptors—specifically the 3-acetyl group in 8 and the heteroaromatic benzothiazol-2-yl ring in 9—suppress non-radiative torsional relaxation and maximize radiative decay. Comparing the structurally analogous amide 3 (6086 counts) and hydrazide 2 (2440 counts) reveals a 2.5-fold brightness enhancement upon replacing –$CONHNH_2$ with –$CONH_2$, attributable to the elimination of flexible N–N bond vibrations and photoinduced electron transfer (PET) quenching from the terminal amino lone pair.

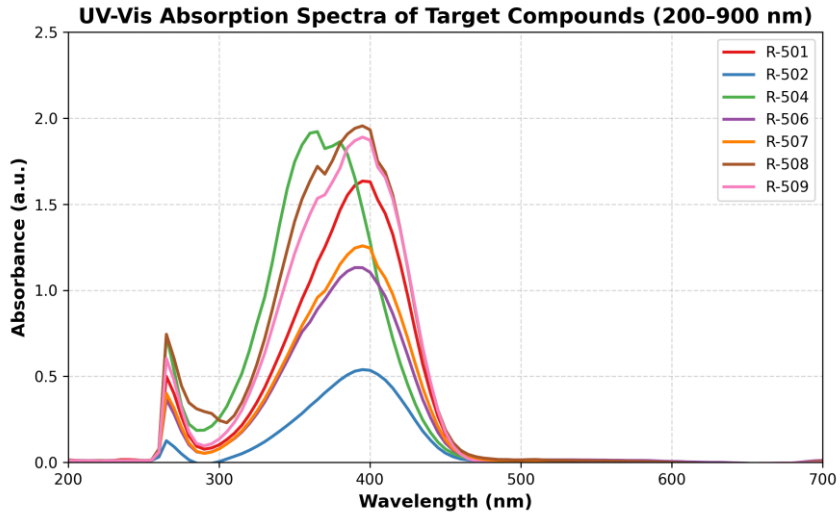

Figure 1. Comparative UV-Vis electronic absorption spectra of compounds 2 (R-501), 3 (R-502), 5 (R-504), 7 (R-506), 8 (R-507), 9 (R-508), and 10 (R-509) in absolute ethanol at 298 K (200–700 nm).

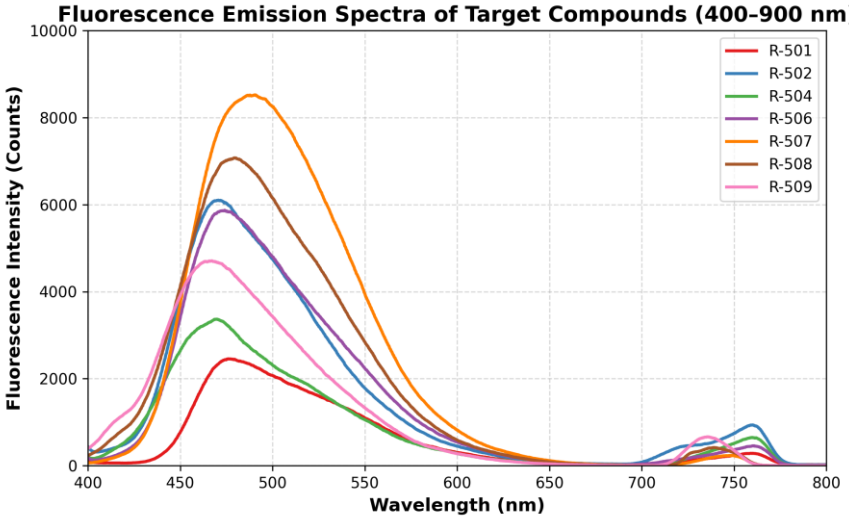

Figure 2. Comparative steady-state photoluminescence emission spectra of compounds 2 (R-501), 3 (R-502), 5 (R-504), 7 (R-506), 8 (R-507), 9 (R-508), and 10 (R-509) in absolute ethanol at 298 K (λex = 365–395 nm).

Whereas compounds 3, 7, 8, and 10 display single-band ICT emission, derivatives 2 (R-501), 5 (R-504), and 9 (R-508) exhibit distinct dual-band luminescence with secondary red-shifted bands at 533.0 nm (1438 counts), 508.6 nm (2089 counts), and 521.6 nm (4807 counts), respectively (Figures 3, 5, and 8). Consistent with established ESIPT-active heterocyclic frameworks [20,23,38,39], photoexcitation of the intramolecularly hydrogen-bonded S(6) chelate ring increases enolic O–H acidity and carbonyl basicity, driving ultrafast excited-state proton transfer (enol* → keto*) to populate a lower-energy tautomeric emitter. In 2 and 9, conformational freedom around the exocyclic C-3 bond further enables relaxation into a twisted intramolecular charge transfer (TICT) state, broadening the secondary emission manifold [18,38].

Primary Stokes shifts across the series range from 72.0 nm (3903 cm^{-1}) for 10 to 104.3 nm (6086 cm^{-1}) for 5, and expand to 126.6–143.5 nm (6145–7728 cm^{-1}) for the secondary phototautomer bands (Table 2). In accordance with photophysical models of ESIPT-mediated Stokes shift expansion [24,40], this wide spectral separation (>70 nm) completely eliminates overlap between the absorption and emission envelopes, suppressing inner-filter artifacts and excitation self-absorption.

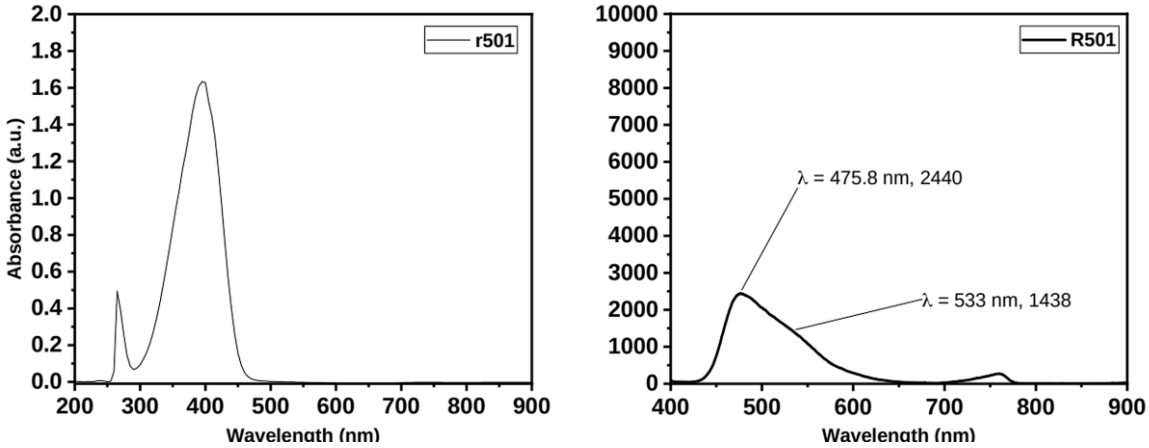

Figure 3. Individual UV-Vis absorption (left, labeled r501) and steady-state fluorescence emission (right, labeled R501; λex = 395 nm) spectra of compound 2 (R-501) in ethanol at 298 K.

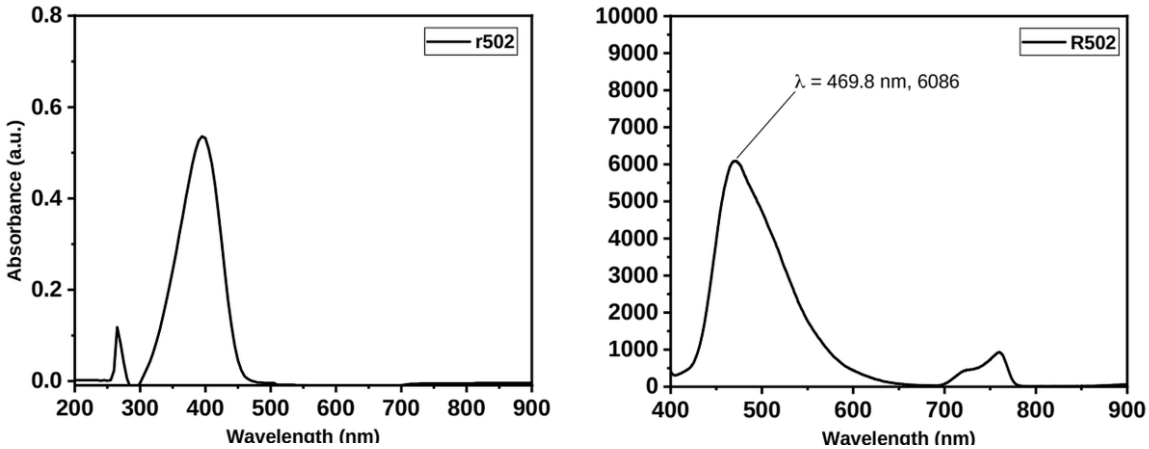

Figure 4. Individual UV-Vis absorption (left, labeled r502) and steady-state fluorescence emission (right, labeled R502; λex = 395 nm) spectra of compound 3 (R-502) in ethanol at 298 K.

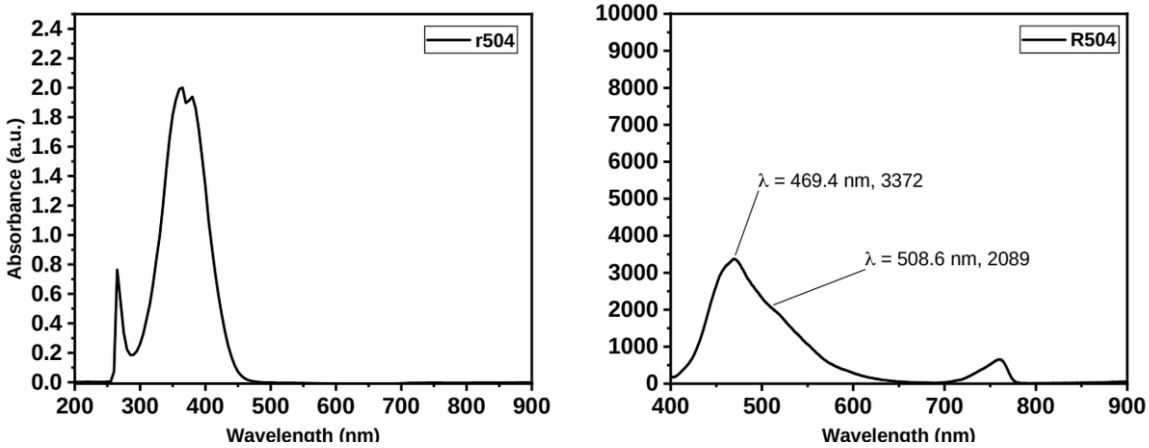

Figure 5. Individual UV-Vis absorption (left, labeled r504) and steady-state fluorescence emission (right, labeled R504; λex = 365 nm) spectra of compound 5 (R-504) in ethanol at 298 K.

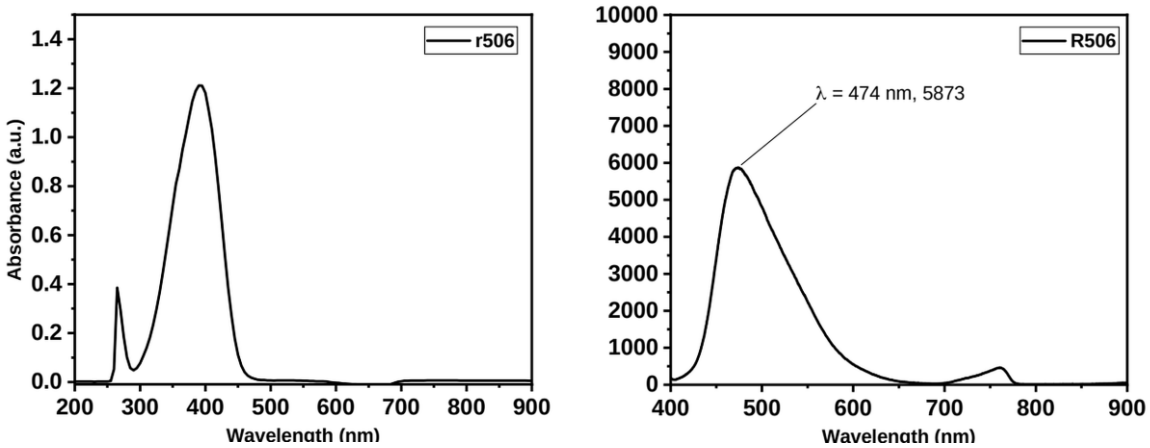

Figure 6. Individual UV-Vis absorption (left, labeled r506) and steady-state fluorescence emission (right, labeled R506; λex = 390 nm) spectra of compound 7 (R-506) in ethanol at 298 K.

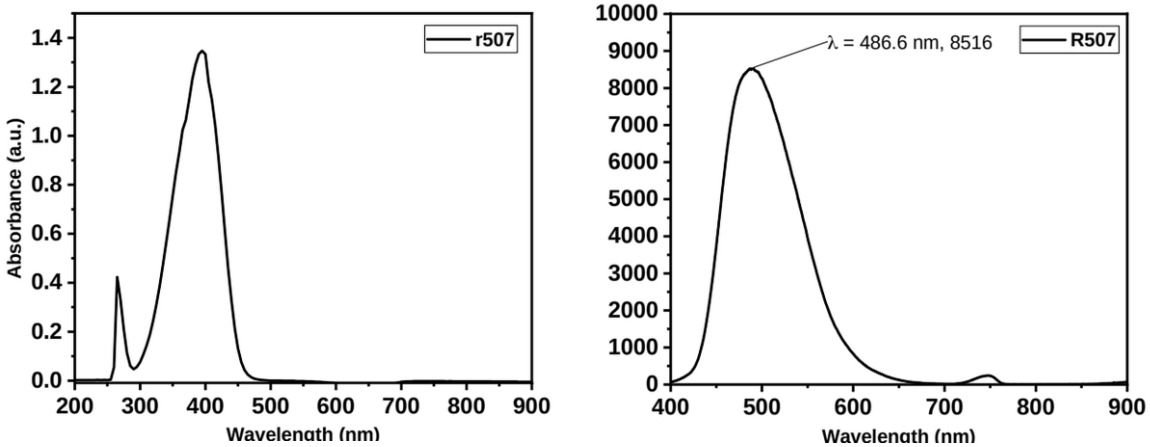

Figure 7. Individual UV-Vis absorption (left, labeled r507) and steady-state fluorescence emission (right, labeled R507; λex = 395 nm) spectra of compound 8 (R-507) in ethanol at 298 K.

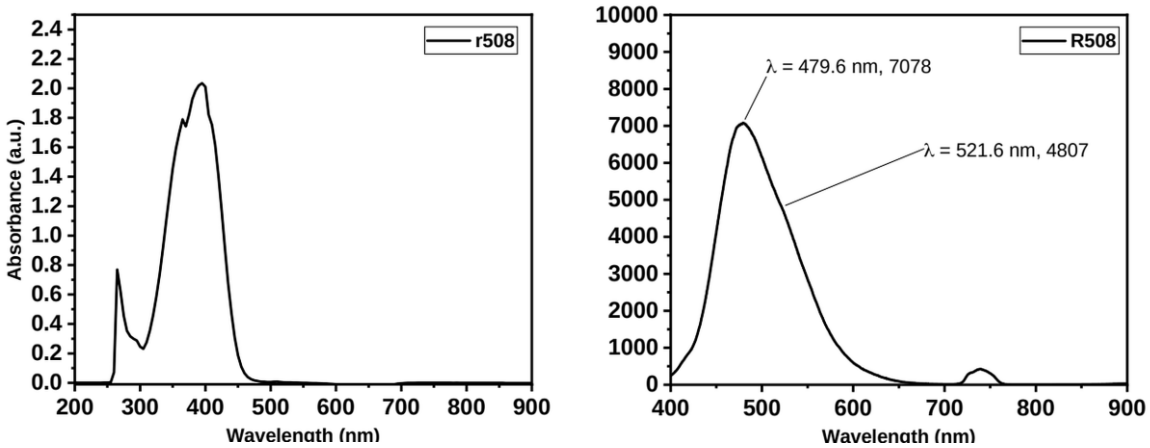

Figure 8. Individual UV-Vis absorption (left, labeled r508) and steady-state fluorescence emission (right, labeled R508; λex = 395 nm) spectra of compound 9 (R-508) in ethanol at 298 K.

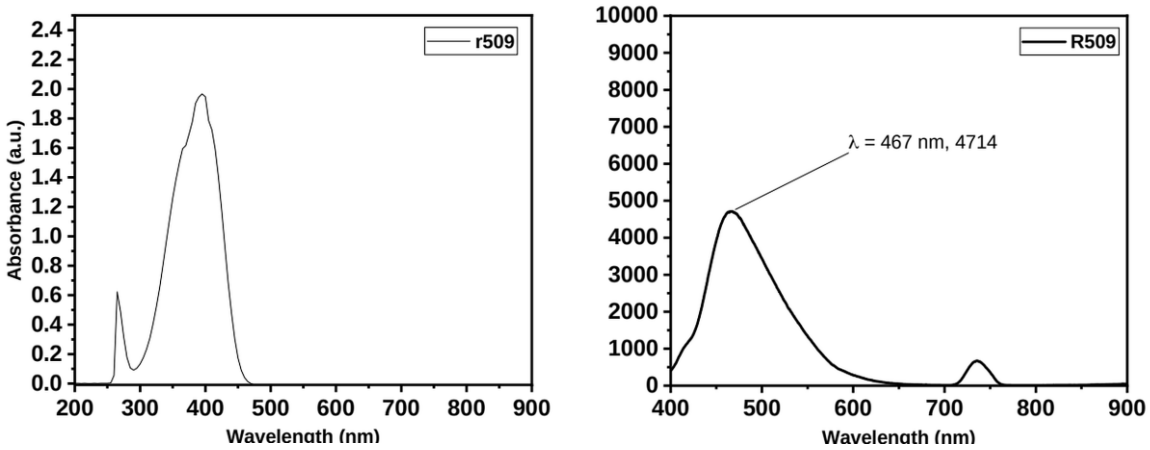

Figure 9. Individual UV-Vis absorption (left, labeled r509) and steady-state fluorescence emission (right, labeled R509; λex = 395 nm) spectra of compound 10 (R-509) in ethanol at 298 K.

3.5. Structure–Property Relationships (SPR) and Prospective Optical Utility

Taken together, the spectroscopic and optical data establish four clear structure–property principles governing the 3,4-dihydrocinnolin-4(1H)-one scaffold, which inform its future development in photonic materials:

- **Conjugation & Planarity Drive Radiative Intensity:** Coplanar, conjugated groups (acetyl in 8 and benzothiazolyl in 9) minimize non-radiative torsional dissipation, maximizing fluorescence intensity (7078–8516 counts).
- **Steric Congestion Modulates Spectral Shifts:** Sterically hindered substituents (chloro/propionyl in 5) distort coplanarity, causing a blue shift of ICT absorption to 365.1 nm and yielding massive Stokes shifts up to 143.5 nm.
- Vibrational Freedom and PET Quenching: Flexible amino-bearing substituents (such as –$CONHNH_2$ in 2) introduce non-radiative vibrational deactivation and PET pathways, lowering emission to 2440 counts compared to 6086 counts in the rigid amide 3.
- S(6) Chelate Architecture and Prospective Utility: Strong RAHB within the S(6) chelate ring drives ESIPT-mediated dual emission and large Stokes shifts (up to 143.5 nm), making these fluorophores promising candidates for future investigation as ratiometric optical probes and luminescent materials.

4. Conclusion

In summary, a divergent, metal-free, and atom-economical synthetic strategy has been developed for the modular preparation of functionalized 3,4-dihydrocinnolin-4(1H)-one fluorophores (2–11) from the versatile diazo linchpin 1. The base-catalyzed tandem cyclocondensation sequences proceed smoothly under mild conditions to afford diverse C-3 quaternary heterocycles and spirocycle 11 in isolated yields of 64–85%. A stepwise reaction mechanism rationalizes the intermolecular nucleophilic addition, intramolecular acyl substitution, and ring dehydration events. Molecular structures were validated by FT-IR, 1H-NMR, 13C-NMR, EI-MS, and elemental microanalyses. Diagnostic 1H-NMR spectroscopy confirmed the formation of a stable S(6) chelate ring via resonance-assisted hydrogen bonding, characterized by a downfield singlet at δ 15.22–16.69 ppm. Photophysical evaluation in ethanol at 298 K revealed substituent-dependent ICT absorption (365.1–395.0 nm) and cyan-to-blue photoluminescence (up to 8516 counts for 8), with derivatives 2, 5, and 9 exhibiting dual-band emission via coupled ESIPT and TICT relaxation dynamics. Large Stokes shifts (72.0–143.5 nm) effectively eliminate self-absorption and inner-filter artifacts. These findings position functionalized 3,4-dihydrocinnolin-4(1H)-ones as promising candidate scaffolds for future exploration in optical sensing, biological imaging, and optoelectronic materials.

References

[1] J. A. Joule, K. Mills, Heterocyclic Chemistry, 5th ed., Wiley-Blackwell, Chichester, 2010.

[2] R. D. Taylor, M. MacCoss, A. D. G. Lawson, Ring system energy and its application in medicinal chemistry, J. Med. Chem. 2014, 57, 5845–5859.

[3] E. Vitaku, D. T. Smith, J. T. Njardarson, Analysis of the structural diversity, substitution patterns, and frequency of nitrogen heterocycles among U.S. FDA approved pharmaceuticals, J. Med. Chem. 2014, 57, 10257–10274.

[4] M. Baumann, I. R. Baxendale, S. V. Ley, N. Nikodemiak, Continuous flow synthesis of functionalized heterocycles, Beilstein J. Org. Chem. 2011, 7, 442–495.

[5] A. R. Katritzky, C. A. Ramsden, J. A. Joule, V. V. Zhdankin, Handbook of Heterocyclic Chemistry, 3rd ed., Elsevier, Oxford, 2010.

[6] G. Hajós, Z. Riedl, Cinnolines, Sci. Synth. 2004, 16, 251–314.

[7] D. E. Ames, H. Z. Kucharska, Cinnolines. Part III. Synthesis of 4-substituted cinnolines, J. Chem. Soc. 1963, 4924–4928.

[8] N. J. Leonard, The chemistry of cinnolines, Chem. Rev. 1945, 37, 269–286.

[9] K. M. Dawood, E. A. Ragab, Synthesis and biological evaluation of novel cinnoline derivatives as anticancer and antimicrobial agents, Bioorg. Med. Chem. 2008, 16, 6433–6441.

[10] A. S. Shawali, M. A. Mosselhi, Chemistry of cinnolines and cinnolinones: synthetic approaches and pharmacological profiles, J. Heterocycl. Chem. 2003, 40, 725–746.

[11] A. Mishra, P. Bäuerle, Small molecule organic semiconductors on the move: promises for photovoltaics, Angew. Chem. Int. Ed. 2012, 51, 2020–2067.

[12] Y. Shirota, H. Kageyama, Charge carrier transporting molecular materials and their applications in devices, Chem. Rev. 2007, 107, 953–1010.

[13] F. Würthner, Dipolar dyes for organic photovoltaics, Acc. Chem. Res. 2016, 49, 868–877.

[14] L. D. Lavis, R. T. Raines, Bright ideas for chemical biology, ACS Chem. Biol. 2008, 3, 142–155.

[15] X. Li, X. Gao, W. Shi, H. Ma, Design strategies for water-soluble small molecule photostable fluorescent probes, Chem. Rev. 2014, 114, 590–659.

[16] Z. Guo, S. Park, J. Yoon, I. Shin, Recent progress in the development of fluorescent probes for bioimaging, Chem. Soc. Rev. 2014, 43, 16–29.

[17] H. Uoyama, K. Goushi, K. Shizu, H. Nomura, C. Adachi, Highly efficient organic light-emitting diodes from delayed fluorescence, Nature 2012, 492, 234–238.

[18] Z. R. Grabowski, K. Rotkiewicz, W. Rettig, Structural changes accompanying intramolecular electron transfer: focus on twisted intramolecular charge-transfer states and structures, Chem. Rev. 2003, 103, 3899–4032.

[19] J. Zhao, S. Ji, Y. Chen, H. Guo, P. Yang, Excited state intramolecular proton transfer (ESIPT) materials: photophysics and applications, Phys. Chem. Chem. Phys. 2012, 14, 8803–8817.

[20] J. E. Kwon, S. Y. Park, Advanced organic luminescent materials: excited-state intramolecular proton transfer (ESIPT) based systems, Adv. Mater. 2011, 23, 3615–3642.

[21] J. Mei, N. L. C. Leung, R. Y. Kwok, J. W. Y. Lam, B. Z. Tang, Aggregation-induced emission: together we shine, united we soar!, Chem. Rev. 2015, 115, 11718–11940.

[22] B. Valeur, M. N. Berberan-Santos, Molecular Fluorescence: Principles and Applications, 2nd ed., Wiley-VCH, Weinheim, 2012.

[23] A. P. Demchenko, K. C. Tang, P. T. Chou, Excited-state intramolecular proton transfer (ESIPT) in chemistry, biology and materials science, Chem. Soc. Rev. 2013, 42, 1379–1408.

[24] L. Wang, W. Chi, W. Sheng, L. Ding, X. Liu, Rational design of large Stokes shift fluorophores via molecular conformation modulation, Chem. Sci. 2020, 11, 10908–10916.

[25] S. G. Agalave, S. R. Maujan, V. S. Pore, Click chemistry: 1,2,3-triazoles as pharmacophores, Chem. Asian J. 2011, 6, 2696–2718.

[26] T. L. Gilchrist, Heterocyclic Chemistry, 3rd ed., Longman, Essex, 1997.

[27] V. von Richter, Ueber Cinnolinderivate, Ber. Dtsch. Chem. Ges. 1883, 16, 677–683.

[28] R. Stoermer, O. Gaus, Synthesen von Cinnolinen und ihren Derivaten, Ber. Dtsch. Chem. Ges. 1912, 45, 3104–3114.

[29] P. W. Neber, H. Bossert, Über neue Bildungsweisen des Cinnolins, Liebigs Ann. Chem. 1935, 518, 274–283.

[30] W. Borsche, W. Scriba, Untersuchungen über Cinnoline. I. Mitteilung, Liebigs Ann. Chem. 1939, 540, 83–98.

[31] J. S. Yadav, B. V. S. Reddy, K. S. Rao, M. S. Rao, InCl3-catalyzed facile synthesis of 3-substituted cinnolines, Tetrahedron Lett. 2008, 49, 614–617.

[32] A. C. Chen, L. De Luca, P. D. Renzi, G. Giacomelli, Microwave-assisted direct synthesis of cinnoline derivatives, J. Org. Chem. 2007, 72, 6310–6313.

[33] K. Suzuki, A. Kobayashi, S. Kaneko, K. Takehira, T. Yoshihara, H. Ishida, Y. Shiina, S. Oishi, S. Tobita, Photophysical properties of 1,2-diazine and diazanaphthalene fluorophores, Phys. Chem. Chem. Phys. 2009, 11, 9850–9860.

[34] G. Gorski, P. Gawrys, S. Krol, Tuning intramolecular charge transfer in heterocyclic fluorophores, Dyes Pigm. 2021, 185, 108892.

[35] M. H. Helal, M. A. Salem, M. M. El-Sawy, Synthesis and photophysical characterization of novel heterocyclic azo dyes with massive Stokes shifts, Spectrochim. Acta Part A 2022, 270, 120815.

[36] H. M. E. Hassaneen, T. A. Farghaly, Synthesis and spectroscopic investigation of novel cinnoline-based fluorophores, RSC Adv. 2023, 13, 21450–21462.

[37] R. M. F. Batista, S. P. G. Costa, M. M. M. Raposo, Synthesis and optical properties of new push-pull heterocyclic chromophores, Tetrahedron 2007, 63, 4258–4265.

[38] T. Mutai, H. Tomoda, T. Ohkawa, Y. Yabe, K. Araki, Switching of dual emission in ESIPT-active heterocyclic materials, J. Chem. Soc. Perkin Trans. 2 2001, 1047–1052.

[39] J. Saltiel, D. F. Sears, J. O. Choi, Tautomeric dynamics and excited-state proton transfer in hydrogen-bonded chelate rings, J. Am. Chem. Soc. 2001, 123, 740–749.

[40] J. Catalan, On the origin of the large Stokes shift in ESIPT dyes: a comprehensive photophysical assessment, Phys. Chem. Chem. Phys. 2014, 16, 12744–12758.